Research Article

Chemical Review and Letters
journal homepage: www.chemrevlett.com
ISSN (online): 2645-4947 (print) 2676-7279

V_2O_5/ZnO/Pd nanocomposites: Preparation, characterization and studying the photocatalytic activity against malachite green

Inam Joudah Radhi[1,*], Aula M. Al Hindawi[1], Hanan Qais AL-Masoudi[1], Noorhan Ali Hamza[1], Zahraa M.Abd Al-Aama[1], Mohammed Ali Hasan[1]

[1]*Department of Chemistry, College of Education for Pure Science, University of Karbala, Karbala, Iraq.*

ARTICLE INFO

Article history:
Received 8 March 2025
Received in revised form 22 April 2025
Accepted 22 April 2025
Available online 10 May 2025

Keywords:
Ternary nanocomposite
Photocatalyst
ZnO
Malachite green dye

ABSTRACT

A novel porous Vanadium pentoxide\Zinc Oxide\Palladium ternary nanocomposite (V_2O_5\ZnO\Pd) was synthesized by photoreduction method. Many techniques were used to characterize the prepared nanocomposite. Binary phase nanocomposites were identified using XRD analysis. The diffraction peaks could be assigned to two crystal phases of hexagonal structure of ZnO and orthorhombic structured of vanadium pentoxide V_2O_5, suggesting the successful incorporation of ZnO and V_2O_5 in the composite. Transmission electron microscopy (TEM) and field emission scanning electron microscopy were used to examine the morphology. The results suggest that V_2O_5/ZnO/Pd nanocomposite has the ability to remove organic contaminants from wastewater and soil pollution treatments. Finally, the nanocomposite 96% efficiency of the photo degradation of dye after 100 min under visible light. The ground-state structures were optimized using density functional theory (DFT), with equilibrium geometries and frontier molecular orbital surfaces, including the highest occupied molecular orbital (HOMO) and the lowest unoccupied molecular orbital (LUMO), determined accordingly. The stability of the ground-state structures was corroborated by a frequency analysis carried out at the same computational level, which verified the lack of imaginary frequencies. The excitation energies of the singlet states were computed based on the optimized ground-state geometries using time-dependent density functional theory (TD-DFT),utilizing the identical functional and foundational set. Along with their configuration interaction descriptions and oscillator strengths, this method yielded the permitted vertical electronic excitation energy, which correlate to absorption energies in the UV/Vis spectral range.

1. Introduction

Industrialization has shown many advantages in human's life style, such as the development of medicine, agriculture efficiency and growth of economy. Numerous negative effects of the industrial revolution include dangers to plant life, climate change, deforestation, global warming, and pollution of the air, soil, and water, which leads to the loss of numerous plant and animal species as well as respiratory illnesses, malignancies, and harm to prenatal health [1]. As a result, a lot of study has been done on the recovery and reuse of contaminated water, which offers a special and practical chance to supplement conventional water supplies. Organic dyes are among the types of pollutants produced by industrial wastewater from printing, photography, painting, leather, and textiles. Researchers are particularly interested in the presence of textile dyes such as malachite green (MG) in wastewater because these dyes are not biodegradable and have negative environmental effects. As a result, many purification methods, including ozonation, adsorption and chlorination, have been suggested as solutions to this problem. Such methods have been extensively used in the past, however, they have a number of drawbacks. Photodegradation was widely used as an alternative way to treat and remove dyes. Metal oxide nanoparticles have been used as a photocatalyst to eliminate MG dye from water. It was found that by mixing biosynthesized ZnO nanoparticles with appropriate amount of MG dye the removal efficiency is 99% after irradiation for 40 min [2]. Xu's group used Ag-Mn oxide nanoparticles to study the

* Corresponding author E-mail: anaam.j@uokerbala.edu.iq
https://doi.org/10.22034/crl.2025.511273.1557

photodegradation of MG dye from an aqueous solution. According to their findings, Ag-Mn oxide nanoparticles had strong broken down and photocatalytic activity 92% of the dye in 120 min. Dye degradation increases with extended irradiation times. Additionally, a greater catalyst dosage led to a higher proportion of dye degradation. Beyond wastewater remediation, nanoparticles have also proven highly effective as catalysts in multicomponent organic reactions due to their high surface area [3, 4], tunable active sites, and efficient charge transport; these very attributes underpin their strong performance as photocatalysts for dye degradation. Researchers have recently utilized binary and ternary composites at the nanoscale level to break down the environmental pollutants such as dyes and drugs. Vanadium pentoxide (V_2O_5) has been widely studied as a visible light active catalyst for the photodegradation of organic contaminants due to its low band gap energy of approximately 2.2 eV [5] During photocatalytic process, the photogenerated electron-hole pairs are recombination quickly and as a result reducing the degradation of impurities. Coupling with other semiconductor with large band gap has been introduced to increasing the life-time of the electron-hole pairs, leading to enhancement in photocatalytic activity. In previous studies, different semiconductors have been coupled with vanadium oxide such as $V_2O_5/BiVO_4$, V_2O_5/Al_2O_3 and V_2O_5/SiO_2 to improve its ability to degraded the impurities [6]. Computational modeling is crucial for revealing how pollutants adsorb and degrade on metal-oxide nanocatalysts [7]. By clarifying band alignment, adsorption energetics at facets/defects, and pathways to reactive oxygen species, it identifies the rate-controlling steps. Combined with adsorption isotherms/kinetics and experiments, these insights guide rational tuning of catalyst composition, morphology, and defect density to suppress e−/h+ recombination and maximize removal efficiency. In this work, n-type semiconductor ZnO was selected as a component of the ternary nanocomposite because of its broad band-gap energy (3.3 eV), superior electron mobility, high optical transparency, and ambient luminescence capability,hopefully this coupling could enhance the photocatalytic activity of vanadium oxide to be used in breaking the unwanted dyes.

2. Materials and Methods

Highly pure materials, including zinc oxide with V_2O_5 nanoparticles, were purchased from Alpha Chemika. Palladium chloride $PdCl_2$ was purchased from Sigma-Aldrich.

2.1. Synthesis of ternary V_2O_5\ZnO\Pd nanocomposite

Binary nanocomposite of V_2O_5\ZnO NPs was first synthesized using low-cost photoreduction method. First, 100 milliliters of deionized water were used to dissolve two grams of V_2O_5\ZnO nanoparticles.

Thereafter, 5 mL of $PdCl_4$ (0.01) M solution was added drop wise to V_2O_5 solution, the mixture was agitated for 15 minutes. The surface of mixture was then exposed to nitrogen gas for 20 min under continuous stirring. The mixture was mixed with 2 mL methanol and irradiated with light (UVA LED lamp with intensity of 1.71 $mW.cm^{-2}$) under continuous magnetic for 12 hours of stirring. To create the ternary V_2O_5\ZnO\Pd nanocomposite, Figure 1 illustrates how the mixture was filtered, repeatedly cleaned with deionized water, then dried at 80°C for a whole day.

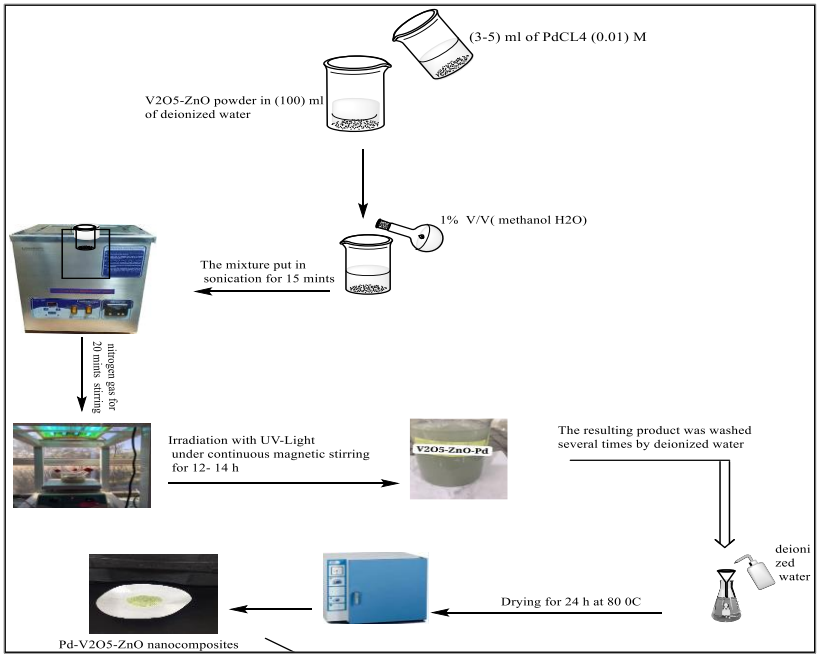

Fig. 1. Diagram illustrating the photoreduction procedure used to create the ternary V2O5\ZnO\Pd nanocomposite.

2.2. Preparation of ternary nanocomposite\MG solution

A standard solution of MG dye was prepared by dissolving 0.2 g in 100 mL of deionized water. Sample was stirred at a speed of 4000 tr/min for different time (15 to 120 min) prior to filtering. UV-Vis spectrophotometer was used to record the wavelength (λmax) of MG dye and it was found 617 nm as shown in Figure 2(a). The solution was then irradiating for 120 minutes using philips mercury lamp UVT (A) which was placed in a home-made photoreactor as shown in Figure 2(b).

3. Results and Discussion

3.1. X-Ray Diffraction (XRD)

Two different phases for the ternary nanocomposite have been observed as shown in Figure 3. One of them belonging to the hexagonal structure of ZnO according to JCPDS card no. 75-0457 and The JCPDS card number 01-1136 indicates that the other is well indexed to the orthorhombic structured V2O5 (α-V_2O_5 phase as it formed at room temperature) [8]. No further impurities, such as VO_3 or\and V_2O_3, were found in the XRD pattern of the prepared nanocomposite, suggesting that the final product have only the distinctive diffraction peaks of V_2O_5 and ZnO. However, no peak was observed for Pd indicating the dispersion of Pd ion through the lattice of the nanocomposite [9].

3.2. Fourier transforms infrared (FTIR) Spectroscopy

The FTIR spectrum for V_2O_5\ZnO\Pd nanocomposite was recorded within the range of (400 -4000) cm^{-1} as shown in Figure 4. Absorption peak appeared on 575 cm^{-1} is assigned to Zn-O bond (Metal-oxide). Peaks appeared at 476 and 712 cm^{-1} are assigned to the asymmetric stretching modes V-O and V-O-V, respectively [10]. Absorption peak centered at 1010 cm-1 corresponds to V=O group [1, 13]. The bending and stretching vibrations of O-H are responsible for the peak at (3429) cm^{-1}[11].

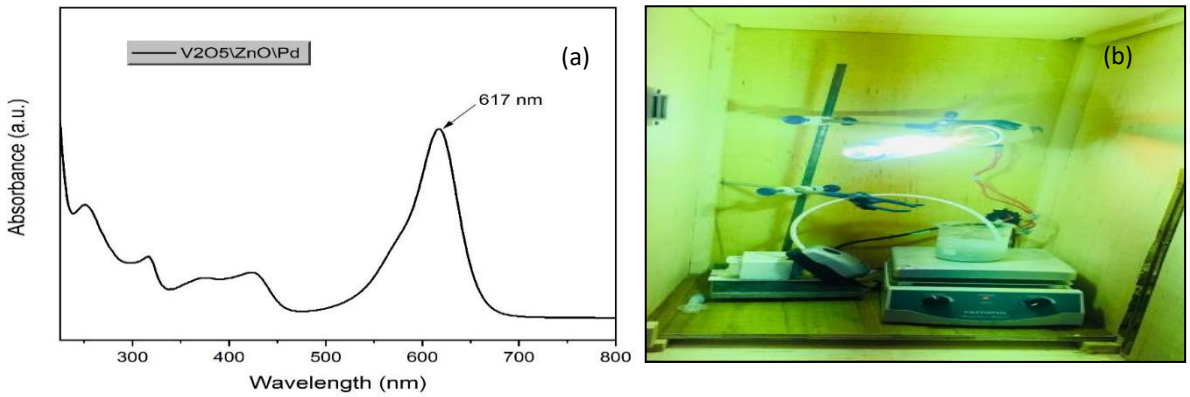

Fig. 2. UV-Vis spectrum showing the λmax of MG dye at 617 nm (a) and home-made photoreactor equipped with philips mercury lamp UVT (b).

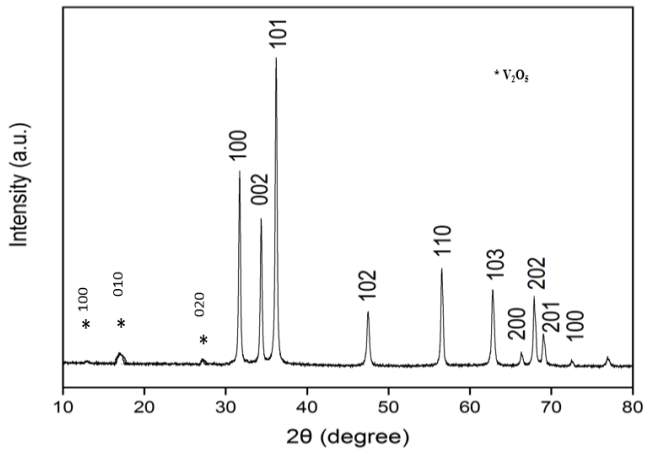

Fig. 3. XRD pattern for the prepared nanocomposite

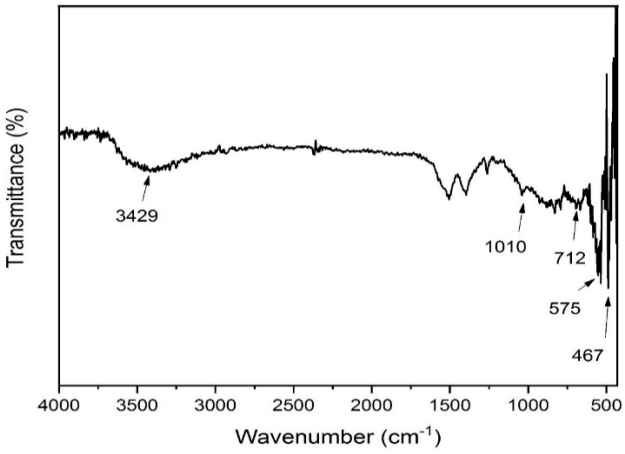

Fig. 4. FTIR spectrum for V_2O_5\ZnO\Pd nanocomposite formed through photoreduction method

3.3. Field Emission-Scanning Electron Microscopy (FE-SEM)

The structural properties of synthesized V_2O_5\ZnO\Pd nanocomposite was studied by field emission scanning electron microscopy (FE-SEM) [12]. Figure 5 shows that the nanocomposites have spherical shape with the appearance of some agglomerated particles, which could be related to the lack of stabilizing and\or capping agent which can help in reducing the agglomeration of particles through providing electrostatic repulsion. The size of these particles was calculated using image program and it was found that the average diameter is 49.21 nm.

With an overall size of nearly a micron, the other population c. It appears that the flower-like structure is related to V_2O_5's innate propensity to form monolayers.

consists of "flower-like" nanostructures. The flower like structure seems to be linked to the natural tendency of V_2O_5 to grow as a monolayer. The inset in Figure(5) shows the selected-area diffraction It appears that the flower-like structure is related to V_2O_5's innate propensity to form monolayers. n pattern of the V_2O_5\ZnO\Pd NPs representing the nanocrystalline behaviour consistent with the XRD results.

3.4. Transmission Electron Microscopy (TEM)

Both size and shape of V_2O_5\ZnO\Pd nanocomposite was investigated using transmission electron microscopy images (TEM). TEM images in Figure 6 show that the majority of particles are spherical in shape with an average diameter of 47 nm which is quite close to that measured with FE-SEM [13, 14].

Transmission Electron Microscopy (TEM) analysis of the nanostructures (NSs) showed that the "nearly-spherical" NPs were adopting an α-phase V2O5, whilst the "flower-like" type NSs were adopting the β-phase V_2O_5.

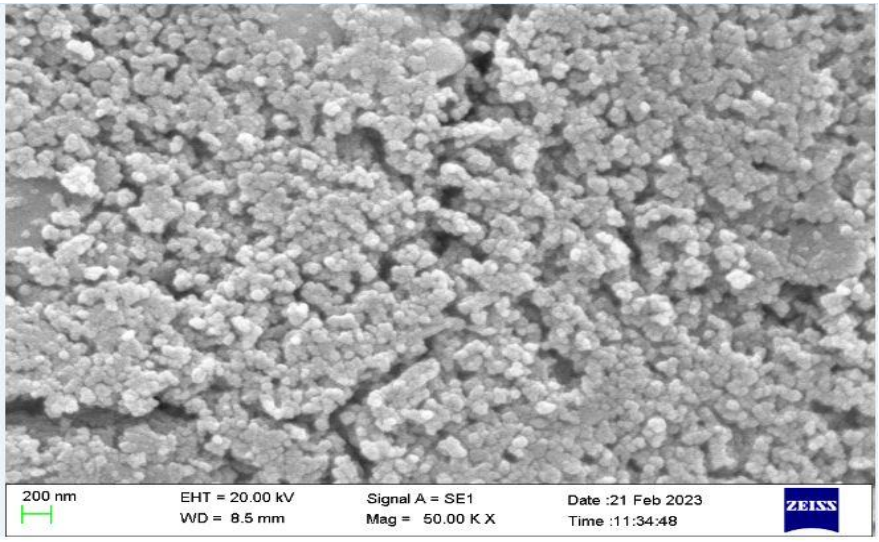

Fig. 5. FE-SEM image for V_2O_5\ZnO \Pd nanocomposite

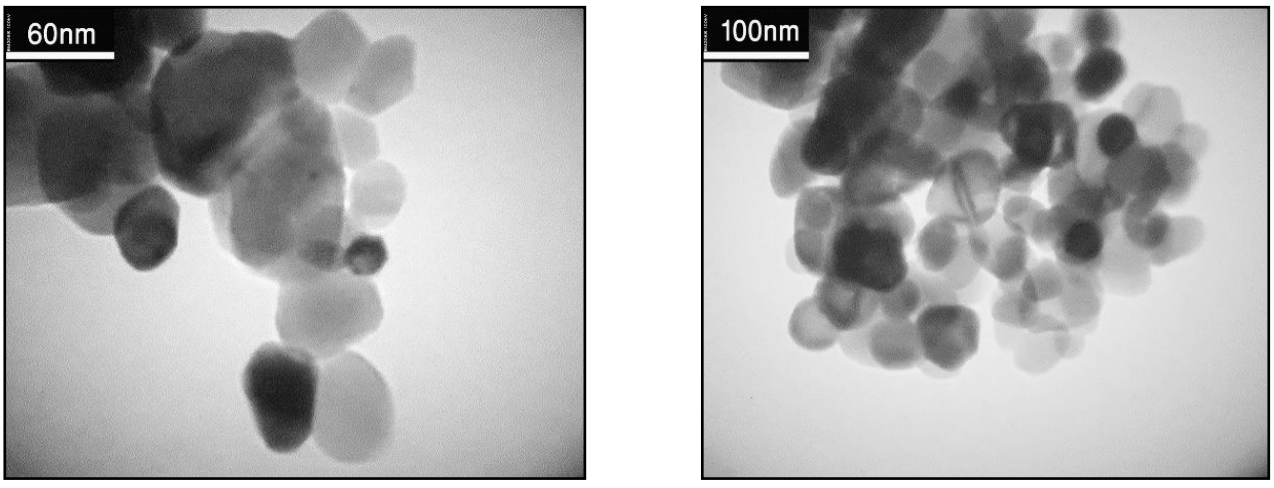

(a) (b)

Fig. 6. TEM photographs of (a) and (b) from (60 to 100) nm respectively of V_2O_5\ZnO \Pd nanocomposite.

3.5. Photocatalytic Degradation

In this experiment the photocatalytic activity of V_2O_5\ZnO\Pd nanocomposite was examined by mixing 0.3 g of the composite with (10 and 15) mg/L of MG dye. One of the most important factors in overcoming all quantity barriers to full molecular transfer between the solid and aqueous phases is the primary concentration. Under UV light, the MG dye at different concentrations (10–15 mg/L) in the presence of 0.3 g of V_2O_5\ZnO\Pd nanocomposite influenced the catalyst's photolysis efficiency [15]. The optimal MG dye concentration was reached after 100 minutes of exposure to UV light, and the absorption was evaluated (Figure 7). Consequently, the nanocomposite's ideal concentration is between 10 and 15 mg/L (96%).

The Photo degradation efficiency was calculated using the following Eq. 1 [16].

Photo Degradation Efficiency (PDE)

$$(\%) = (1 - C^t/C^o) \times (100\%) \quad (1)$$

Where C^o is the initial MG concentration and Ct is the concentration following the irradiation period. The best removal efficiency was found to be 96%.

Yin Haihong, et al found that the rate of accelerated photodegradation of methylene blue is high when the dye mixed with V_2O_5/ZnO Nanocomposite compare with the one mixed with bare ZnO nanoparticles. They attributed that to the stronger localization of plasmonic near-field effects, which expanded the light absorption zone, as a consequence the efficient electron-hole separation at the interfaces between V_2O_5 and Au and ZnO [17]. The proper mechanism for the photocatalytic activity of the ternary nanocomposite was suggested as follows: Pd improves the visible-light response by SPR, V_2O_5 absorbs visible light and produces more charge carriers, and ZnO absorbs UV light and produces electron-hole pairs [18]. Charge separation is made easier by the heterojunction between ZnO and V_2O_5. Pd nanoparticles decrease recombination by acting as electron sinks [19]. As a consequence, O_2 is reduced by electrons (e^-) to $O_2^{-}\bullet$ (superoxide radicals) and H_2O is oxidized by holes (h^+) to OH• (hydroxyl radicals) [20, 21]. Organic contaminants (dies) are broken down by these radicals into CO_2 and H_2O as seen in Figure 8.

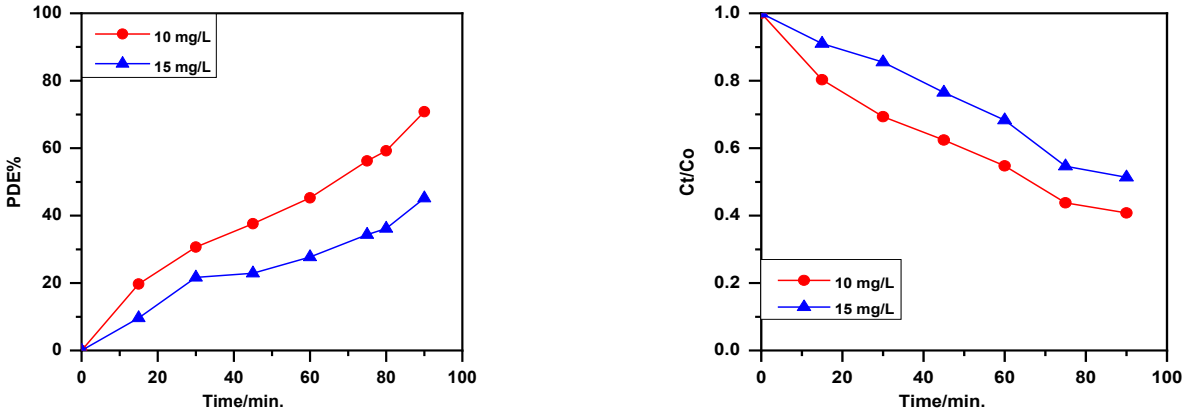

(a) (b)

Fig. 7. The PDE% after treating the MG dye with V_2O_5\ZnO \Pd nanocomposite (a), and the concentration of the dye after irradiation time (b).

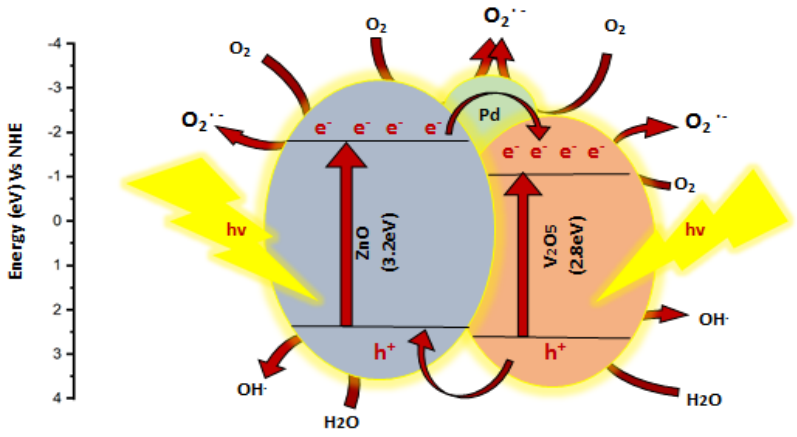

Fig. 8. Schematic diagram showing the photocatalytic ability of V_2O_5\ZnO \Pd nanocomposite.

3.6. Surface area analysis

The Brauner, Emmitte and Telar (BET) analysis is not consistent with the low mass concentrations of nanoparticles, which are typically in the range of 0.1 mg/m3 or less [17]. The V_2O_5/ZnO/Pd NPs sample has surface areas of 20.747 m^2 g-1, according to Table 1. BET measurement shows that the V_2O_5/ZnO/Pd NPs have total pore volumes of 0.1501 cm^3/g. Additionally, when the nanomaterials exhibit in the 28.941 range after being inoculated with Palladium chloride ($PdCl_2$) via the photo deposition procedure, the pores' diameter reduces, measured BET surface area of the sample V_2O_5/ZnO/Pd NPs was smaller (20.747 m^2/g)which can be correlated to the fact that the method of preparation helped to form a nanocomposite distinguished by its physical and chemical properties, indicating that the high surface area and high mesopore volume fraction of the V_2O_5/ZnO/Pd NPs supports could be used to decorate the supports with Pd nanocatalysts even when the interior region is not being used efficiently [22]. Therefore, the mesopore structure and large surface area would improve the electrochemical active sites, which would improve the oscillator strengths and catalytic configuration interaction (CI) descriptions Figure 9.

3.7. Computational Method

Ground states (GS) were optimized using Density Functional Theory (DFT) with the B3LYP functional as implemented in the Gaussian 09 software package [23]. Equilibrium geometries and frontier orbital surfaces (HOMO and LUMO) were calculated using the 6-311G (d,p) basis set. The lack of imaginary frequencies in the GS was validated by frequency analysis conducted at the same computational level [24].

The energies of the excited singlet states (ES) were calculated from the GS geometries using time-dependent density functional theory (TD-DFT) [25], using the same base and functional set. This technique produced the permitted vertical electronic excitation energy, which in turn produced the UV/Vis absorption energies.

To determine the maximum wavelength of ZnO, and V_2O_5, Figure 10 and 11 show the ultraviolet-visible (UV-Vis) absorption spectra of ZnO and V_2O_5 spanning the wavelength range of 173-512 nm.

The maximum wavelengths (λmax) corresponding to the highest absorption in the UV-Vis spectrum were identified for ZnO, and V_2O_5 at 512 nm, and 173 nm, respectively[26,27]. With an energy gap of -2.64 eV, these transitions result from the change from the highest occupied molecular orbital (HOMO) to the lowest unoccupied molecular orbital (LUMO), as seen in Figure 12. The calculations also revealed one additional forbidden transition with marginal intensities: from the HOMO to the LUMO of ZnO with an energy splitting of -1.67 Ev [28,29].

Table 1. Surface area measurements of V_2O_5/ZnO/Pd nanocomposite

Surface physical parameters	V_2O_5/ZnO/Pd nanocomposite
BET surface area ($a_{s, BET}$)	20.747 m^2/g
Average pore diameter	28.941 nm
Total Pore volume (p/p^0) = 0.979	0.1501 cm^3/g
Type of pore	Micro-pores
C	-51.372
V_m	4.7668 [cm^3 (STP) g^{-1}]

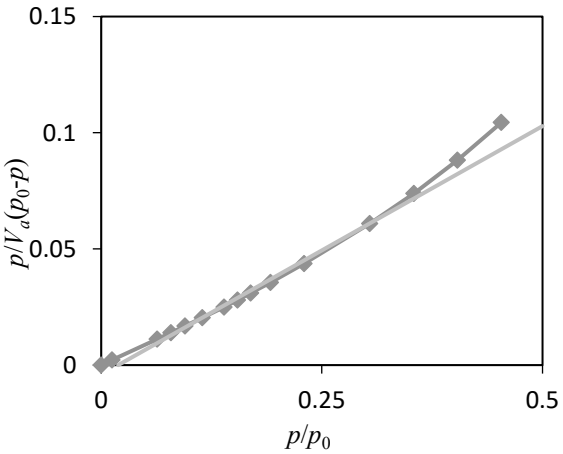

Fig. 9. BET adsorption–desorption isotherm of V_2O_5/ZnO/Pd NPs

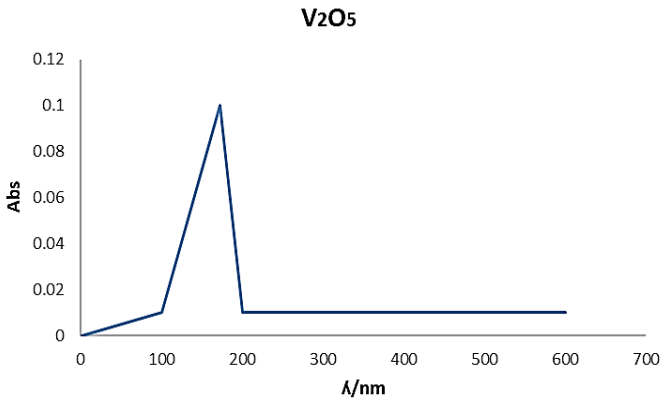

Fig. 10: A-UV-Visible absorption spectra of V_2O_5.

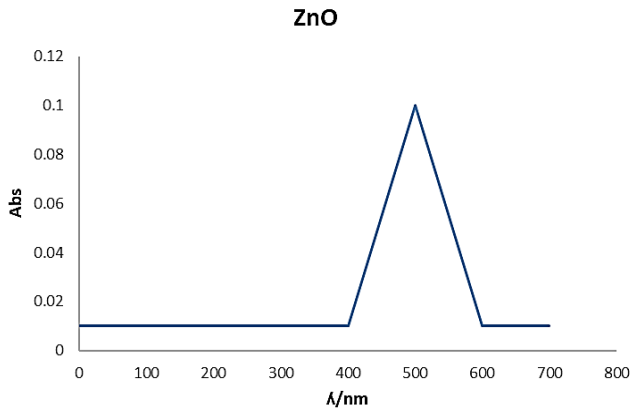

Fig. 11. A-UV-Visible absorption spectra of ZnO.

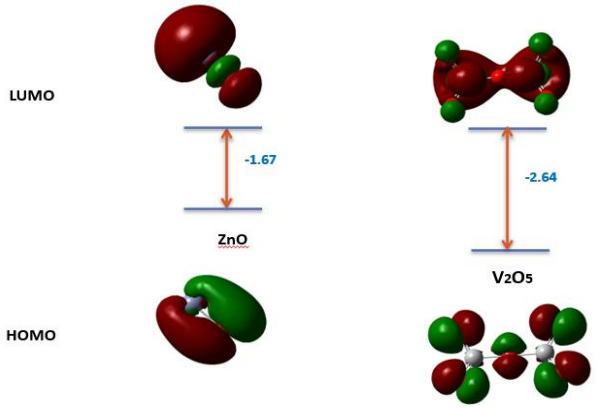

Fig. 12. the energy difference (eV) between the frontier orbitals for the synthesize compounds.

4. Conclusion

Photoreduction method was used to produce V_2O_5\ZnO\Pd nanocomposite. This composite exhibit two phases according to the XRD pattern one is identified as the hexagonal structure of ZnO and the other as the orthorhombic structured V_2O_5. The V_2O_5/ZnO/Pd nanocomposite's excellent light absorption, improved radical production, and effective charge separation contribute to its exceptional photocatalytic activity. It is therefore a viable option for sustainable pollutant degradation and environmental remediation. It was found that after 100 minutes of elimination under UVA LED, about 96% of the dye was successfully destroyed. A frequency analysis performed at the same computational level verified the stability of the ground states by confirming the absence of imaginary frequencies. The excitation energies of the singlet states were determined based on the optimized ground-state geometries using time-dependent density functional theory (TD-DFT), employing the same functional and basis set. This approach enabled the calculation of allowed vertical electronic excitation energies, which correspond to absorption energies in the UV/Vis spectral region, along with their associated configuration interaction descriptions and oscillator strengths.

References

[1] (a) A. M. Al Hindawi, I. Joudah, S. Hamzah, Z. Tarek, Plant extract: safe way for fabrication silver nanoparticles. In: *IOP Conf. Ser.: Mater. Sci. Eng.*, Vol. 571, IOP Publishing (2019) 012069; (b) A. Q. Abed, A. M. A. Hindawi, H. F. Alesary, Synthesis and characterization of zinc sulfide nanomaterials for removal methylene blue dye from aqueous solution. In: *AIP Conf. Proc.*, Vol. 2591, AIP Publishing (2023) 020054; (c) R. S. Al-Shemary, I. J. Mahdi, N. N. Hussein, A. G. Hadi, S. J. Baqir, Sustainable dye removal using synthesized chitosan for reactive black 5 adsorption. *Chem. Res. Technol.*, 2 (2025) 38–44. https://doi.org/10.22034/chemrestec.2025.523466.1050; (d) A. J. Al-lamei, A comparative efficiency study of two adsorbent materials to remove of organic fluorine compounds from aqueous solutions. *J. Chem. Lett.*, 6 (2025) 188–195. https://doi.org/10.22034/jchemlett.2025.509156.1285; (e) N. S. Yapo, K. E. Adou, J. Ano, D. N. Nonh, K. B. Yao, Adsorption of fluoride ions on hydroxyapatite-modified Corbula trigona shell waste: Effect of coexisting anions, temperature and regeneration. *J. Chem. Lett.*, 4 (2023) 95–102. https://doi.org/10.22034/jchemlett.2023.393828.1112.

[2] (a) M. S. Hamdy, K. V. Chandekar, M. Shkir, S. AlFaify, E. H. Ibrahim, Z. Ahmad, M. Kilany, B. M. Al-Shehri, K. S. Al-Namshah, Novel Mg@ZnO nanoparticles synthesized by facile one-step combustion route for anti-microbial, cytotoxicity and photocatalysis applications. *J. Nanostruct. Chem.*, 11 (2021) 147-163; (b) M. Hraja, A. Al Hindawi, N. Shiltagh, Investigation of electronic and molecular features of Zn_3S_3/peg4000 nano-composite using the DFT method. *J. Turk. Chem. Soc. A*, 11 (2024) 565-574.

[3] (a) Z. Hossaini, S. Ahmadi, D. Zareyee, S. S. Amiri, Green synthesis of new spiropyrroloisatin and spiroindenopyrroles using biosynthesized CuO/ZnO@MWCNTs nanocatalyst. *Chem. Rev. Lett.*, 7 (2024) 1063–1073. https://doi.org/10.22034/crl.2024.472507.1400; (b) H. Ghavidel, B. Mirza, S. Soleimani-Amiri, M. Manafi, New insight into experimental and theoretical mechanistic study on a green synthesis of functionalized 4H-chromenes using magnetic nanoparticle catalyst. *J. Chin. Chem. Soc.*, 67 (2020) 1856-1876. https://doi.org/10.1002/jccs.20190055467.

[4] (a) S. Soleimani Amiri, Y. Salemi, Novel butane sulfonic acid-functionalized core–shell magnetic nanocatalysts for ultrasound-assisted coumarin synthesis. *New J. Chem.*, 48 (2024) 2299-2310. https://doi.org/10.1039/D3NJ04912D; (b) M. Feizpour Bonab, S. Soleimani-Amiri, B. Mirza, Fe_3O_4@C@PrS-SO_3H: A novel efficient magnetically recoverable heterogeneous catalyst in the ultrasound-assisted synthesis of coumarin derivatives. *Polycycl. Aromat. Compd.*, 43 (2023) 1628-1643. https://doi.org/10.1080/10406638.2022.2032768.

[5] J. Mehta, K. Gupta, S. Lavania, P. Kumar, V. Chaudhary, P. Gupta, Inherent roadmap in synthesis and applications of sustainable materials using oil based and microbial polymers. *Mater. Today Sustainability*, 25 (2024) 100615.

[6] I. J. Radhi, S. Hassan, A. F. Alkaim, Preparation and characterization of ZnO, WO_3/ZnO nanocomposites using hydrothermal method. *J. Nanostruct.*, 13 (2023) 327-334.

[7] (a) S. Soleimani-Amiri, A. Khanmohammadi, E. Vessally, J. Makasana, S. Ballal, R. Panigrahi, et al., Metal–porphyrin functionalized carbon nanocones as promising $COCl_2$ sensors: a DFT and NBO perspective. *Comput. Theor. Chem.*, 1253 (2025) 115457. https://doi.org/10.1016/j.comptc.2025.115457; (b) A. S. Hessen, N. M. A. Alsultany, H. Bahir, A. H. Adthab, S. Soleimani-Amiri, S. Ahmadi, et al., Adsorption of sulfur mustard on the transition metals (TM = Ti^{2+},Fe^{2+},Co^{2+}, Ni^{2+}, Cu^{2+}, Zn^{2+}) porphyrins induced in carbon nanocone (TM-PCNC): Insight from DFT calculation. *J. Mol. Graph. Model.*, 135 (2025) 108928. https://doi.org/10.1016/j.jmgm.2024.108928; (c) V. O. Oninla, K. N. Awokoya, L. C. Overah, J. O. Babalola, A. J. Ademuwagun, A. I. Adetunji, A. M. Ayoola, Fenton's reagent-initiated modification of plantain (Musa paradisiaca) peel biomass – mechanisms of chain propagation and dyes removal from simulated wastewaters. *J. Chem. Lett.*, 5 (2024) 221–235. https://doi.org/10.22034/jchemlett.2024.466424.1206.

[8] (a) Z. T. Turki, A. M. A. Hindawi, N. M. Shiltagh, Fabrication and characterization of cadmium sulfide nanoparticles using chemical precipitation method. In: *AIP Conf. Proc.*, Vol. 2591, AIP Publishing (2023) 020055; (b) R. Saravanan, V. Gupta, E. Mosquera, F. Gracia, Preparation and characterization of V_2O_5/ZnO nanocomposite system for photocatalytic application. *J. Mol. Liq.*, 198 (2014) 409-412.

[9] S. Lavania, J. Mehta, P. Bhardwaj, A. Tripathi, N. Gupta, P. Gupta, Biocomposites: prospects and manifold applications for human and environmental sustainability. *ECS J. Solid State Sci. Technol.*, 12 (2023) 037002.

[10] H. Panchal, K. K. Sadasivuni, A. A. A. Ahmed, S. S. Hishan, M. H. Doranehgard, F. A. Essa, S. Shanmugan, M. Khalid, Graphite powder mixed with black paint on the absorber plate of the solar still to enhance yield: An experimental investigation. *Desalination*, 520 (2021) 115349.

[11] P. Shukla, J. K. Shukla, Facile sol-gel synthesis and enhanced photocatalytic activity of the V_2O_5-ZnO nanoflakes. *J. Sci.: Adv. Mater. Devices*, 3 (2018) 452-455.

[12] S. Yang, H. Wu, Q. Luo, A. M. Al Hindawi, B. Sitorus, A. M. Ellis, J. Yang, Ion-molecule reactions catalyzed by a single gold atom. *Chem. Sci.*, 11 (2020) 8502-8505.

[13] A. H. Wdaah, H. I. Salman, A. A. Balakit, Synthesis and characterization of selenium-polyvinyl alcohol nanoparticles as eco-friendly corrosion inhibitor for carbon steel in 1.0 M H_2SO_4. *Inorg. Chem. Commun.*, 165 (2024) 112505.

[14] A. Ahmed, A. Al Hindawi, N. Shiltagh, Role of manganese ion in tuning the structural and optical properties of silver sulfide nanostructures. *Chem. Rev. Lett.*, 7 (2024) 622-629.

[15] K. E. Yunusov, M. Mirkholisov, N. S. Ashurov, A. Sarymsakov, S. S. Rashidova, Formation of zinc oxide nanoparticles in aqueous solutions of carboxymethylcellulose and their physico-chemical properties. *Polym. Sci. Ser. B*, 66 (2024) 129-137.

[16] I. J. Radhi, S. Hassan, A. F. Alkaim, UV–visible light induced photocatalytic degradation studies of Ag doped ZnO/WO_3 nanoparticles prepared by co-precipitation method. *NeuroQuantology*, 20 (2022) 5233-5240.

[17] H. Yin, K. Yu, C. Song, R. Huang, Z. Zhu, Synthesis of Au-decorated V_2O_5@ZnO heteronanostructures and enhanced plasmonic photocatalytic activity. *ACS Appl. Mater. Interfaces*, 6 (2014) 14851-14860.

[18] K. E. Yunusov, M. M. Mirkholisov, M. A. Azizova, J. Z. Jalilov, S. S. Yarmatov, J. N. Todjiyev, A. A. Sarimsakov, A. A. Atakhanov, J. Guohua, A. A. Rogachev, Advances in the formation and properties of nanofiber biomaterials from polyvinyl alcohol/carboxymethylcellulose/nanosilver systems for medical applications. *Chem. Rev. Lett.*, 8 (2025) 20-38.

[19] H. Panchal, K. K. Sadasivuni, C. Prajapati, M. Khalid, F. Essa, S. Shanmugan, N. Pandya, M. Suresh, M. Israr, S. Dharaskar, Productivity enhancement of solar still with thermoelectric modules from groundwater to produce potable water: a review. *Groundwater Sustain. Dev.*, 11 (2020) 100429.

[20] K. K. Sadasivuni, K. Deshmukh, T. Ahipa, A. Muzaffar, M. B. Ahamed, S. K. Pasha, M. A.-A. Al-Maadeed, Flexible, biodegradable and recyclable solar cells: a review. *J. Mater. Sci.: Mater. Electron.*, 30 (2019) 951-974.

[21] K. Pansal, B. Ramani, K. K. Sadasivuni, H. Panchal, M. Manokar, R. Sathyamurthy, M. Suresh, M. Israr, Use of solar photovoltaic with active solar still to improve distillate output: a review. *Groundwater Sustain. Dev.*, 10 (2020) 100341.

[22] G. Topcu, A. M. Al Hindawi, C. Feng, D. Spence, B. Sitorus, H. Liu, A. M. Ellis, S. Yang, Precision engineering of nano-assemblies in superfluid helium by the use of van der Waals forces. *Commun. Chem.*, 7 (2024) 125.

[23] S. Gnanasekar, P. Sonar, S. M. Jain, S. K. Jeong, A. N. Grace, Performance evaluation of a low-cost, novel vanadium nitride xerogel (VNXG) as a platinum-free electrocatalyst for dye-sensitized solar cells. *RSC Adv.*, 10 (2020) 41177-41186.

[24] I. J. Radhi, A. A. Al-Khafagi, M. K. Kahlol, M. S. Mashkoor, 1,2-Naphthoquinone-4-sulphonate sodium as reagent for spectrophotometric determination of pioglitazone. *Int. J. Drug Deliv. Technol.*, 11 (2021) 165-171.

[25] J. Tirado-Rives, W. L. Jorgensen, Performance of B3LYP density functional methods for a large set of organic molecules. *J. Chem. Theory Comput.*, 4 (2008) 297-306.

[26] M. E. Casida, Time-dependent density-functional theory for molecules and molecular solids. *J. Mol. Struct.: THEOCHEM*, 914 (2009) 3-18.

[27] J. F. Ali, J. I. Radhi, I. H. Salman, A. S. Hassan, Study the efficiency of cement kiln dust waste for removal some dyes. *Chem. Rev. Lett.*, 8 (2025) 187-198.

[28] K. E. Yunusov, et al., Formation, structure, and morphology of nanofiber mat on the base sodium-carboxymethylcellulose/polyvinyl-alcohol/silver nanoparticles composite. *Polym. Adv. Technol.*, 35 (2024) e6496.

[29] K. E. Yunusov, et al., Advances in the formation and properties of nanofiber biomaterials from polyvinyl alcohol/carboxymethylcellulose/nanosilver systems for medical applications. *Chem. Rev. Lett.*, 8 (2025) 20-38.